[Autophagy 5:4, 461-471; 16 May 2009]; ©2009 Landes Bioscience

Research Paper

Mutation at the cargo-receptor binding site of Atg8 also affects its general autophagy regulation function

Kung-Hsien Ho,[1] Hsiang-En Chang[1] and Wei-Pang Huang[1,2,*]

[1]Institution of Zoology; and [2]Department of Life Science; National Taiwan University; Taipei, Taiwan, Republic of China

Key words: autophagy, cargo sorting, membrane trafficking, vesicle formation

Autophagy is a highly conserved degradation pathway for intracellular macromolecules and organelles. Among those characterized autophagy regulators, the ubiquitin-like protein Atg8 is found to be a membrane modifier that both regulates biogenesis of transport vesicles and interacts with the cargo receptor Atg19 for selective autophagic transport of the vacuolar enzyme prApe1 in budding yeast. The role of Atg8 in the enlargement of vesicle membrane during autophagosome biogenesis has been well documented, but how Atg8 coordinates vesicle formation and sorting of selective cargo is largely unknown. Identification of the cargo-receptor binding site of Atg8 would provide information to solve this issue. Here we characterized Atg8 mutants that were defective in interaction with the prApe1 receptor Atg19 and found that the vesicle formation function of these Atg8 mutants was also compromised to different extents. Atg8 mutants with single-residue substitution at the Atg19-binding site were defective in lipid conjugation and/or subcellular localization. Additional Atg8 mutants were found defective in autophagosome formation without affecting their interaction with Atg19, suggesting partially overlapping of the cargo-sorting site and its domains critical for autophagy control. Our observation paves the road for a more comprehensive understanding on how Atg8 coordinates cargo sorting and vesicle formation in selective autophagic pathways.

Introduction

Macroautophagy, a conserved membrane trafficking mechanism in eukaryotic cells and hereafter referred to as autophagy, is known to be highly activated by nutrient starvation stresses to nonselectively deliver macromolecules for lysosomal degradation and recycling.[1] Recent studies have unveiled additional physiological functions of this pathway.[1] For example, exogenously induced autophagy confines and eliminates infection of intracellular pathogens, such as group A Streptococcus, *Mycobacterium tuberculosis* and certain Shigella strain.[2-4] Endogenously generated protein aggregates are ubiquitinated and degraded via the autophagy pathway.[5,6] Many of these newly recognized roles of autophagy rely on efficient mechanisms to sort and load cargo into transport vesicles. However, mechanisms underlying sorting of autophagic cargo remain largely unknown.

Studies in *Saccharomyces cerevisiae* have identified 18 genes required for the execution of autophagy.[7] The protein products of these *ATG* (autophagy-related) genes act jointly to drive de novo formation of cytosolic double-membrane vesicles named autophagosomes, which is the hallmark of this trafficking mechanism.[8] Autophagosomes eventually fuse with lysosomes leading to their demise and degradation of their transport cargo. Among the 18 Atg proteins, two ubiquitin-like conjugation systems collaboratively regulate autophagosome formation. Covalent linkage of Atg8 to isolation membrane, the intermediate structure of autophagosomes, is the direct outcome of actions of the two conjugation systems.[9-11] Nascent Atg8, a ubiquitin-like protein, is made with an arginine residue at its C-terminus, which is quickly cut off by the action of Atg4 protease to expose the penultimate glycine during the priming process. Atg7 and Atg3 subsequently act as the E1-like and E2-like enzymes of this system to catalyze reactions parallel to the ubiquitination modification. Only, the final result is an amide covalent linkage between the Atg8 C-terminal glycine and the polar head amino group of a phosphatidylethanolamine (PE). Lipidated Atg8 (Atg8-PE) coats isolation membrane to facilitate autophagosome formation. Ultimately, Atg8 is released from the cytosolic surface of completely formed autophagosomes via the deconjugation reaction catalyzed by Atg4.[11]

In addition to regulating vesicle formation, Atg8 also facilitates selective cargo transport by autophagy and its related pathway, the cytoplasm to vacuole targeting (Cvt) pathway, in budding yeast.[12] The vacuolar enzyme aminopeptidase 1 (Ape1) is selectively transported by the Cvt pathway or autophagy depending on nutrient conditions. Immediately after their synthesis, precursors of Ape1 (prApe1) quickly assemble into a higher order Cvt protein complex, which also contains another selective transport cargo α-mannosidase and the cargo receptor Atg19.[13,14] By interaction with Atg11 and Atg8, Atg19 facilitates sorting and delivering the Cvt complex to the pre-autophagosomal structure (PAS), where the Cvt and autophagic transport vesicles are assembled.[15,16] Studies of the prApe1 transport have shed light on the molecular mechanisms of cargo sorting in selective autophagic pathways.

*Correspondence to: Wei-Pang Huang; Department of Life Science; National Taiwan University; Taipei, Taiwan 10617 Republic of China; Tel.: +886.2.3662506; Fax: +886.2.23673374; Email: wphuang@ntu.edu.tw

Submitted: 09/07/08; Revised: 12/05/08; Accepted: 12/23/08

Previously published online as an *Autophagy* E-publication:
http://www.landesbioscience.com/journals/autophagy/article/7696

In mammalian cells, autophagic elimination of protein aggregates seems to parallel the yeast Cvt pathway in many aspects. Presence of cargo evokes transport without the need of starvation stimulus for the Cvt pathway and mammalian selective autophagy may operate in a similar manner. Both of their selective cargoes organize into higher order protein structures. Although information is limited, their cargo sorting machineries also reveal some level of similarity. Protein aggregates in mammalian cells are marked by ubiquitins. The poly-ubiquitin-binding protein p62 recognizes this complex as a selective cargo and mediates its clearance by interaction with microtubule-associated protein 1-light chain 3 (LC3), one of the mammalian homologs of yeast Atg8, which reveals the cargo-sorting function of LC3.[17] Other mammalian Atg8 homologs include Golgi-associated ATPase enhancer of 16 kDa (GATE-16), and gamma-aminobutyric-acid-type-A (GABA) receptor associated protein (GABARAP). All these three Atg8 homologs have been confirmed subjected to lipidation processing.[18] Furthermore, GABARAP regulates intracellular trafficking of $GABA_A$ receptors.[19,20] These data suggest that the post-translational modification and their roles in cargo-sorting may be well conserved between Atg8 and at least some of its mammalian homologs. Therefore, analyzing the interaction between Atg8 and Atg19 in details could potentially provide a molecular model of the cargo-sorting mechanisms of selective autophagy.

Atg8 plays two roles in regulation of selective autophagic transport, one to facilitate the assembly of vesicles and the other to mediate selective cargo sorting. Currently, it is not clear if the two functions of Atg8 correlate with each other. One major reason is because the cargo-receptor binding site in Atg8 is still not known. On the contrary, two previous studies have identified several residues of Atg8 important for vesicle formation.[21,22] Whether those vesicle formation-defective Atg8 mutants are incapable of interaction with the Cvt complex, however, has not been tested. In this study, we applied the structural information of LC3, GATE-16 and GABARAP to analyze candidate residues of Atg8 for interaction with Atg19. Our results indicate that Arg28, Tyr49 and Leu50 of Atg8 are involved in both interaction with Atg19 and regulation of general autophagic transport. Additionally, substitution of residue Lys48 or Leu55 of Atg8 retards autophagy transport at two different steps without compromising their interaction with Atg19. Our study has identified the cargo-sorting site of one member of the ubiquitin-like Atg8 family proteins. Overlapping in residues required for the two functions of Atg8 suggests some level of crosstalk or interference may exist between them.

Results

In *S. cerevisiae*, efficient transport of the selective cargo prApe1 by Cvt vesicles or autophagosomes requires the interaction between the cargo receptor Atg19 protein and the membrane modifier Atg8. The C-terminal region of Atg19 is previously mapped responsible for this interaction.[12] Further characterization of the interaction between Atg19 and Atg8 could provide valuable information for understanding the cargo-sorting mechanism of selective prApe1 transport.

Atg8 loses interaction with C-terminal charge-reversed Atg19 mutants. A distinct feature of the C terminus of Atg19 is its highly concentrated acidic residues. Because this region is responsible for interaction with Atg8, we suspected that these acidic residues of Atg19 could mediate ionic interactions with oppositely charged

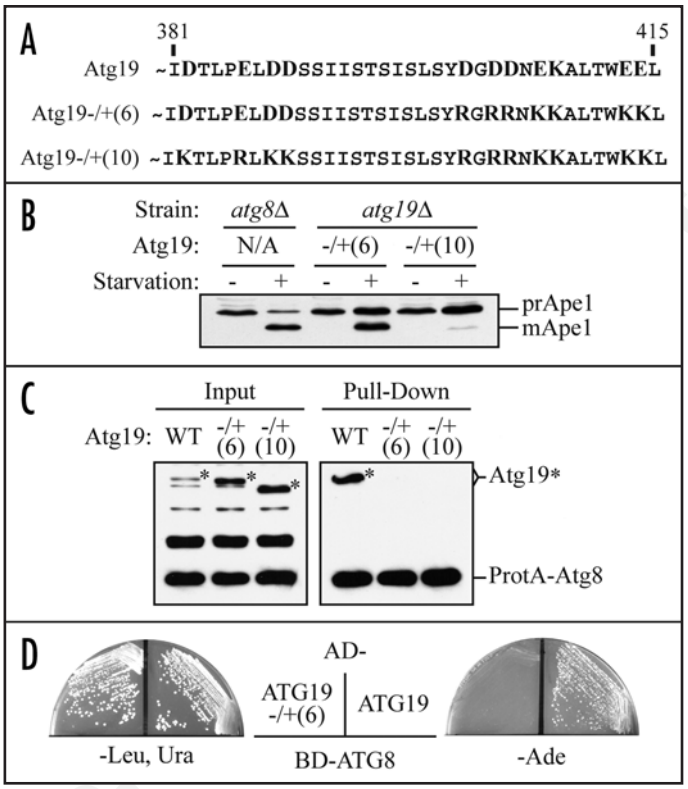

Figure 1. Atg8 interacts with an Atg19 C-terminal acidic domain. (A) Sequence alignment of the C-terminal acidic domain of wild-type Atg19 and the charge-reversed Atg19 variants. Acidic residues are shown in red color and positively charged residues are shown in blue color. (B) Cells of an *atg8*Δ strain or *atg19*Δ cells expressing the indicated charge-reversed Atg19 variants were collected from mid-log phase cultures or after 4 hours of starvation in SD-N medium. Immunoblotting analysis against Ape1 detected its processing statuses. (C) Total cell lysates of *atg19*Δ cells expressing Protein A epitope-tagged Atg8 (ProtA-Atg8) and the indicated Atg19 proteins were prepared from mid-log phase cultures. Human IgG-coated Dynabeads were used to precipitate ProtA-Atg8 and associated proteins. Immunoblotting analyses using anti-Atg19 antibodies detect Atg19 variants. (D) Plasmids expressing the Gal4 transcription activation domain (AD)-tagged Atg19 or $Atg19^{-/+(6)}$, and the DNA-binding domain (BD)-tagged Atg8 were transformed into an *atg19*Δ two-hybrid test strain. The interaction between Atg19 variants and Atg8 were tested by plating transformants on an adenosine dropout selection plate (-Ade). Successful transformation of the indicated plasmids to yeast cells were confirmed by plating cells on a leucine and uracil double dropout selection plate (-Leu, Ura).

surface residues of Atg8. To test this speculation, charge-reversed Atg19 variants with six and ten acidic residues at the C terminus substituted with positively charged residues, named $Atg19^{-/+(6)}$ and $Atg19^{-/+(10)}$, respectively, were prepared (Fig. 1A). Expression of these Atg19 variants did not complement the prApe1 processing defect seen for an *atg19*Δ strain maintained in nutrient-rich medium (Fig. 1B). Starvation treatment is known to partially reverse prApe1 transport defect in *atg8*Δ cells.[29] Expression of $Atg19^{-/+(6)}$ in *atg19*Δ cells partially restored prApe1 transport under starvation stress while cells expressing $Atg19^{-/+(10)}$ still accumulated prApe1 as the major form (Fig. 1B), suggesting that $Atg19^{-/+(6)}$ might have lost interaction with Atg8, whereas $Atg19^{-/+(10)}$ might have additional defects, such as inability to interact with Atg11, another Atg protein important for prApe1 transport.[16] To examine their interaction with Atg8, cell lysates from *atg19*Δ cells expressing either wild-type Atg19 or

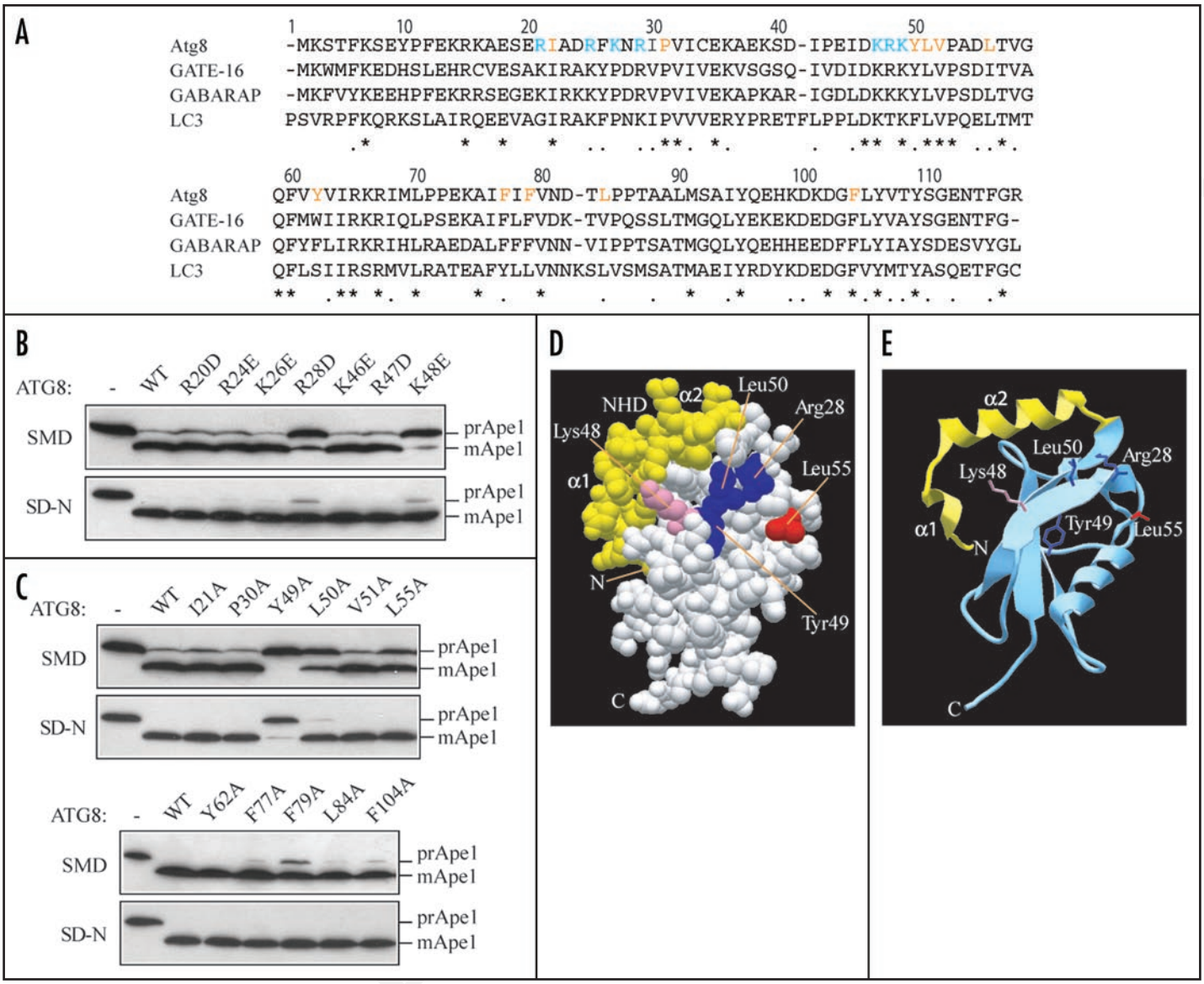

Figure 2. Selection of Atg8 mutants with prApe1 transport defect. (A) Multiple sequence alignment of Atg8, LC3, GATE-16 and GABARAP. Stars and dots denote identical and similar residues, respectively. Positive and hydrophobic residues of Atg8 tested in this study are labeled in blue and orange, respectively. The residue number of Atg8 was labeled above its sequence. Only partial sequences of GATE-16, GABARAP and LC3 are presented. (B and C) Maturation of prApe1 was analyzed in *atg8*Δ cells expressing (B) the indicated charge-reversed Atg8 variants or (C) the indicated Atg8 variants with a single hydrophobic residue substitution. Cultures grown to mid-log phase in nutrient rich media (SMD) were harvested or shifted to nitrogen starvation media (SD-N) for 4 hours and then subjected to immunoblotting analysis using anti-Ape1 antibodies. (D and E) Homology-modeling structure of Atg8. Side chains of residues involved in the maturation of prApe1 were labeled. NHD, α1, and α2 represented the N-terminal helical domain and the comprising first two α-helixes of Atg8. N and C represent the N- and C-terminus of Atg8, respectively.

the charge-reversed Atg19 mutants together with Atg8 tagged at the N-terminus with the IgG-binding domain of protein A (ProtA-Atg8) were used for affinity purification of Atg8 and its associated proteins. Unlike wild-type Atg19, both forms of charge-reversed Atg19 variants were not co-isolated with ProtA-Atg8 (Fig. 1C). A yeast two-hybrid analysis confirmed that the charge-reversed Atg19 variant did not interact with Atg8 (Fig. 1D). These results supported that electrostatic forces between Atg19 and Atg8 are involved in their interaction.

Isolation of Atg8 mutants defective in prApe1 transport. To further study the role of Atg8 in autophagic cargo sorting, we then intended to identify the Atg19-binding site of Atg8. Based on the resolved structure of GATE-16, a mammalian homolog sharing 56% sequence identity with Atg8, a structure of Atg8 was predicted by homology-modeling (Fig. 2D and E). Several residues conserved among Atg8 and its mammalian homologs form a positively charged patch on protein surface (Fig. 2A), which was predicted to be a protein-protein interaction region of GATE-16 responsible for interaction with its downstream effectors.[30] In addition, another potential protein binding site was also predicted for GATE-16 and LC3.[30,31] These regions of Atg8 and several partially exposed hydrophobic residues in the vicinity were hence tested for requirement in prApe1 transport and interaction with Atg19. In addition, we also examined their selective cargo transport abilities for several Atg8 variants that

have been previously identified defective in autophagy regulation.[21,22]

Cells expressing a variant of Atg8 with either a charge-reversed residue or a hydrophobic residue substituted by alanine were examined for prApe1 maturation (Fig. 2B and C). Under nutrient-rich vegetative growth condition (SMD), prApe1 is transported by the Cvt pathway. Atg8 variants with substitutions at Arg28, Lys48, Tyr49, Leu50 or Leu55 were defective in prApe1 transport revealing the potential involvement of these residues for interaction with Atg19. Starvation treatments induce autophagy activities leading to partial bypass of the requirement of Atg8 for prApe1 transport and autophagosome formation.[16,29] We tested the effect of nitrogen starvation treatment (SD-N) and found that the defects for all the Atg8 variants except Atg8^{Y49A} were reversed, indicating a more severe defect for Atg8^{Y49A}.

Atg8 residues required for interaction with Atg19. Atg8 mutants defective in prApe1 transport may result from either cargo sorting or general vesicle formation defects. To identify residues directly involved in interaction with Atg19, the IgG-binding domain of protein A-tagged Atg8 variants were prepared for copurification analyses. Consistent with our hypothesis, Atg8^{R28D} with a charge-reversed residue was inefficient in pulling down of Atg19 and prApe1, indicating ionic interactions between Atg8 and Atg19 (Fig. 3A). Unlike the charge-reversed construct, Atg8^{R28A} with a neutral substitution complemented prApe1 transport defect of *atg8*Δ cells under growth condition (data not shown). Because Atg8^{R28D} still supported nonspecific autophagic transport (see below), indicating its structure was not significantly altered due to the single residue substitution, these data suggested the charge of this residue instead of the specific amino acid identity was important for Atg19 and Atg8 interaction. Interestingly, Atg8^{Y49A} and Atg9^{L50A} were also found defective in copurification of the Atg19-prApe1 complex. Although not being continuous with Arg28 in the primary structure, Tyr49 and Leu50 are in close proximity to Arg28 and partially exposed to the surface of Atg8 (Fig. 2D and E). These copurification results were further confirmed by a yeast two-hybrid analysis experiment (Fig. 3B). Our data together suggested that the Atg19-binding site of Atg8 comprises at least Arg28, Tyr49 and Leu50.

We next examined if these three residues of Atg8 were specific for interaction with Atg19 without affecting the assembly of transport vesicles. Progression of the autophagy pathway eventually leads to Atg8-PE, which has been trapped inside of autophagosomes, being delivered to and degraded in vacuoles.[23] In cells expressing GFP-Atg8, the accumulation of the free form of GFP in vacuoles due to its resilience to degradation allows monitoring the progression

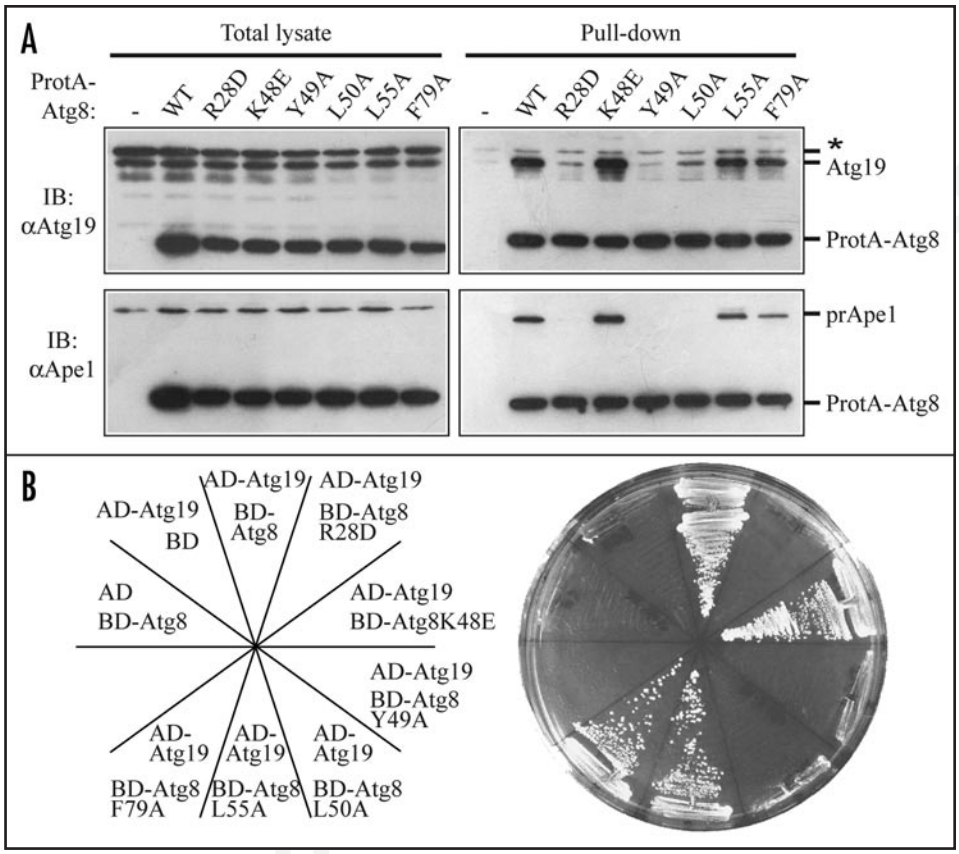

Figure 3. Residue Arg28, Tyr49 and Leu50 of Atg8 constitute the Atg19-binding site. (A) Total cell lysates of *atg1*Δ*atg8*Δ cells expressing Protein A epitope alone (-) or tagged versions of the indicated Atg8 variants were prepared from mid-log phase cultures. Human IgG-coated Dynabeads were used to precipitate Prot.A-Atg8 and associated proteins. Immunoblotting analyses using anti-Ape1 or anti-Atg19 antibodies detect the copurified prApe1 and Atg19. A cross-reacting signal nonspecifically co-isolated with ProtA-Atg8 is labeled with a star (*). (B) Plasmids expressing the Gal4 AD, the Gal4 BD, or the indicated fusion proteins were transformed into an *atg8*Δ two-hybrid test strain. The interaction between Atg19 and Atg8 variants were tested by plating transformants on a histidine dropout selection plate with 3 mM of 3-AT.

of the autophagy pathway.[32] Once the cells are shifted to starvation conditions, the accumulation rate of free GFP in GFP-Atg8^{R28D} transformants was similar to that of cells expressing wild-type GFP-Atg8, whereas those of GFP-Atg8^{Y49A}- and GFP-Atg8^{L50A}-expressing cells were delayed suggesting that these two Atg8 mutants are partially defective in autophagy (Fig. 4A).

To further quantify the autophagic defects of these Atg8 variants, the alkaline phosphatase (ALP) enzyme assay was conducted. Due to its lack of the signal peptide, the truncated version of ALP with 60 residues deleted from its N-terminus (Pho8Δ60) is not translocated into the endoplasmic reticulum (ER) like the full-length ALP does and results in accumulation of enzymatically inactive Pho8Δ60 in cytoplasm, which can only be delivered to and then activated in vacuoles by nonspecific autophagic transport during starvation. Enzymatic assay of Pho8Δ60 activity can thus quantitatively evaluate autophagy activities.[28] Atg8^{Y49A} and Atg8^{L50A} indeed only restored limited abilities to activate Pho8Δ60 in starved *atg8*Δ cells, while Atg8^{R28D} showed an activity of more than 60% of the wild-type Atg8 (Fig. 4B). In addition, autophagic recycling of intracellular materials enables cells to survive longer in a nutrient deprived environment.[33] Survival rates are hence related to the abilities to conduct

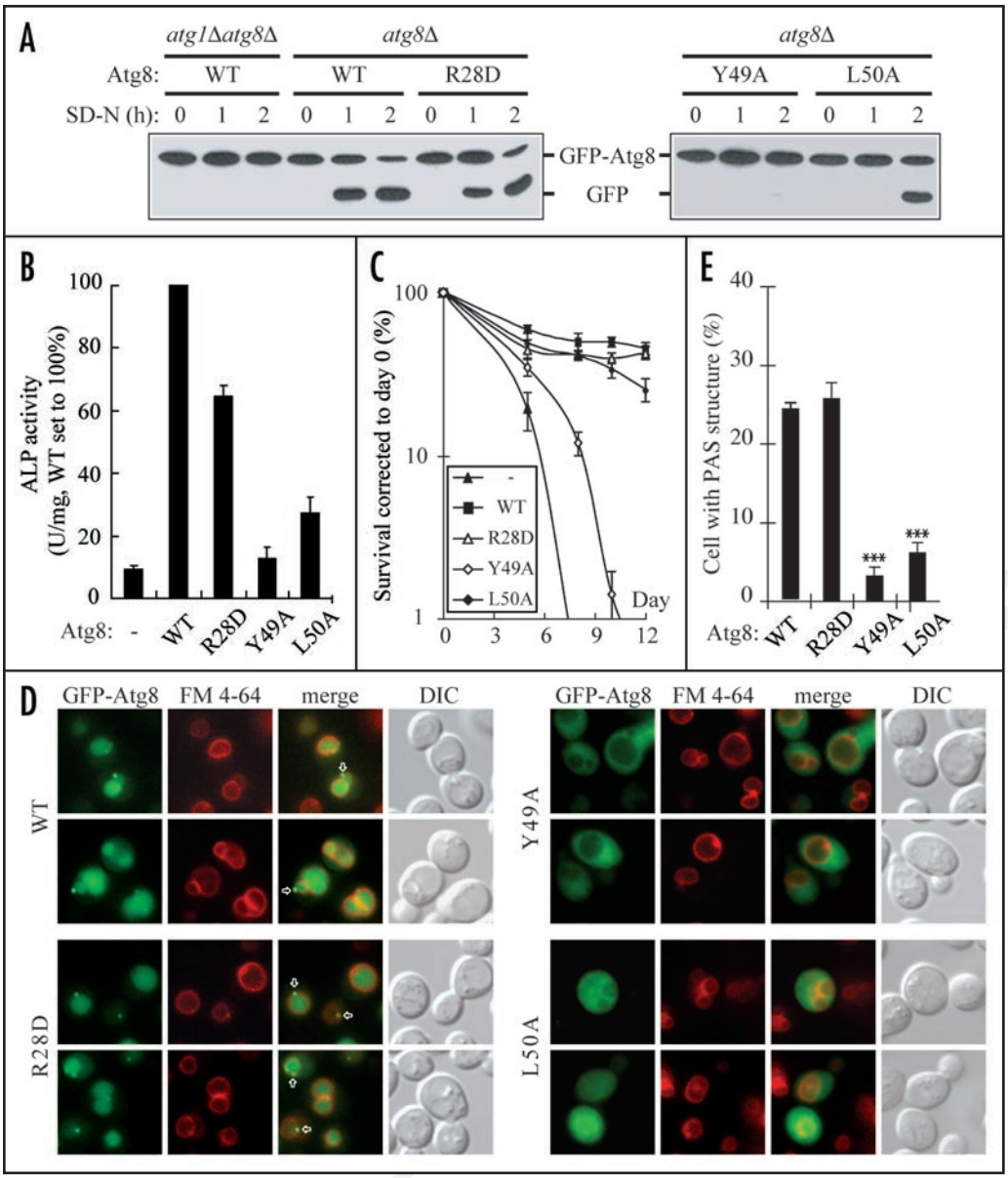

Figure 4. Characterization of Atg8^{R28D}, Atg8^{Y49A} and Atg8^{L50A} for autophagy activities. (A) Plasmids expressing GFP fusion of wild-type or mutant Atg8 were transformed into *atg8*Δ or *atg1*Δ*atg8*Δ cells. Mid-log phase cultures and cells starved in SD-N for 1 or 2 hours were subjected to immunoblotting analysis using anti-GFP antibodies. (B) An *atg8*Δ strain harboring an empty vector or plasmids expressing Atg8 variants were prepared for ALP assay after 4 hours of starvation. The ALP activity of cells expressing wild type Atg8 was set to 100%. Error bars represent the standard deviations of three trials. (C) Mid-log phase *atg8*Δ cells holding an empty vector or plasmids expressing Atg8 variants were maintained in SD-N for survival rate test. Equal amounts of cell aliquots were taken out at the indicated dates and plated on YPD plates for colony counting. The survival rate on day 0 (prior to starvation treatment) of each transformants was set to 100%. (D) Mid-log phase cells as described in (A) were stained with FM 4–64 to label their vacuoles and then switched to SD-N for 2 hours before image acquiring. Arrows indicate PAS localized GFP-Atg8 variants. The percentages of cells exhibiting PAS-localized GFP-Atg8 variant signals were quantified (E). Error bars represent the standard deviations of three trials. In each trial, at least 100 cells were counted for each variant. Asterisks represent statistical difference between variants and wild type (***$p < 0.0001$).

autophagy. Consistent with the other results, Atg8^{Y49A}-expressing cells died earlier than wild-type cells or cells containing Atg8^{R28D} or Atg8^{L50A} (Fig. 4C). Collectively, mutations of residue Arg28, Tyr49 or Leu50 resulted in mild to severe autophagic defects in addition to their abrogated interaction with Atg19. Among these three residues, Arg28 seems to be more specifically involved in Atg8-Atg19 interaction and plays a less important role in regulation of autophagy.

Atg8^{Y49A} fails to form conjugation with PE. The impaired properties of these Atg8 variants affecting autophagy regulation were next analyzed. Wild-type Atg8 regulates vesicle formation at the PAS. Therefore, if Atg8 variants were successfully recruited to the PAS was first examined by fluorescence microscopy. GFP-Atg8^{R28D} behaved like wild type locating at the PAS and accumulated inside vacuoles after starvation treatment (Fig. 4D and E). Consistent with the previous results, GFP-Atg8^{Y49A} and GFP-Atg8^{L50A} were less frequently accumulated in vacuoles indicating their severe autophagic defects. Additionally, they could hardly be observed localizing at the PAS, which implies a defect in PAS recruitment.

Recruitment of Atg8 to the PAS requires PE conjugation at its C-terminus.[9,10] Thus, being absent at the PAS may be resulted from abolished lipidation. To analyze the accessibilities to conjugation modification, Atg8 variants were examined by immunoblotting analyses. The level of high mobility Atg8-PE increased after shifting cells to starvation medium (Fig. 5A). The generation of Atg8^{R28D}-PE and Atg8^{L50A}-PE seemed to be normal, whereas Atg8^{Y49A}-PE was hardly detected. Further, Atg8 proteins in *atg1*Δ*atg8*Δ cells were examined in order to eliminate the effect of vacuolar degradation caused by autophagy flux. Signals of Atg8^{Y49A}-PE were still low indicating a genuine conjugation defect for this Atg8 mutant.

Formation of Atg8-PE requires first removal of its C-terminal arginine residue by Atg4, and then subsequent reactions in a ubiquitination-like manner catalyzed by Atg7and Atg3. Because Atg8^{Y49A} was inefficiently recruited to the PAS and defective in lipid conjugation, its enzymatic processing for PE conjugation was examined. Nascent Atg8^{Y49A}-EGFP and Atg8^{L50A}-EGFP fusion proteins with C-terminal GFP tag were processed normally as its wild-type counterpart indicating normal C-terminal priming (Fig. 5B). Copurification

and the yeast two-hybrid analysis results suggested that Atg8^{Y49A} and Atg8^{L50A} interacted with the E1-like Atg7 normally (Fig. 5C and data not shown). Unfortunately, antiserum for detecting the E2-like Atg3 is not available in our laboratory and both N- and C-terminal epitope-tagging compromise Atg3 function (data not shown). Thus, the interaction between Atg3 and Atg8^{Y49A} was not tested in this study. Together, mutations of residue Tyr49 but not of residue Leu50 of Atg8 impaired its lipidation although these two residues were both important for efficient PAS targeting.

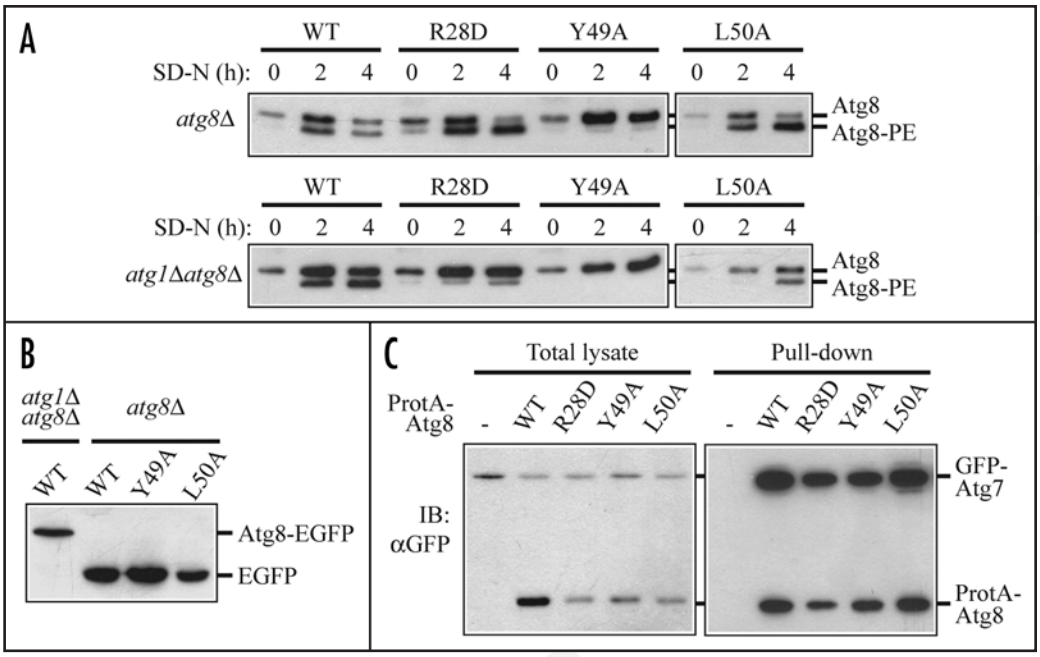

Figure 5. Analysis of Atg8^{R28D}, Atg8^{Y49A} and Atg8^{L50A} for processing defects. (A) Mid-log phase *atg8*Δ cells expressing Atg8 variants were harvested or switched to SD-N for 2 or 4 hours. Cells were then subjected to Atg8 immunoblotting analysis for detecting lipidation. (B) Cells of *atg8*Δ or *atg4*Δ*atg8*Δ strains expressing the C-terminal EGFP fusion of wild-type or mutant Atg8 were harvested from SMD and analyzed by immunoblotting using anti-GFP antibodies. (C) Cell lysates prepared from an *atg1*Δ*atg8*Δ strain expressing GFP-Atg7 and Protein A epitope alone (-) or the indicated ProtA-tagged Atg8 variants were incubated with human IgG-coated dynabeads at 4°C overnight. Then the washed beads were eluted with Laemmli sample buffer and subjected to immunoblotting analysis using anti-GFP antibodies.

Atg8^{K48E} and Atg8^{L55A} are defective in autophagy. Atg8^{K48E} and Atg8^{L55A} isolated by our mutagenesis analysis showed a defect in prApe1 transport but could interact with Atg19 normally (Figs. 2B and C; and 3). Assays for autophagy efficiency by accumulation of free form of GFP cut off from GFP-Atg8 variants and cell survival analyses indicated mild autophagy defects for Atg8^{K48E} and Atg8^{L55A} (Fig. 6A and B). Interestingly, GFP-Atg8^{K48E} and GFP-Atg8^{L55A} were found mostly restricted to the PAS instead of being transported into vacuoles in starved cells (Fig. 6C and D), indicating that substitution of residue Lys48 or Leu55 of Atg8 affects some events downstream to their PAS recruitment.

Atg8^{L55A} accumulates in PE-conjugated form. Once being recruited to the PAS, Atg8 subsequently mediates the assembly of autophagosomes, and then is deconjugated from PE by cytosolic Atg4 to allow fusion of autophagosomes with vacuoles. Therefore, the steady-state ratio of PE-conjugated versus free Atg8 in cells is regulated by conjugation, deconjugation and vacuolar degradation via autophagy flux events. In *atg8*Δ cells, Atg8^{K48E}-PE and Atg8^{L55A}-PE existed in ratios higher than that of wild-type Atg8 (Fig. 7A). The slightly accumulated Atg8^{K48E}-PE phenotype comparing to cells with wild-type Atg8 was no longer obvious in an autophagic deficient *atg1*Δ*atg8*Δ strain, implying that its accumulation in an *atg8*Δ strain is likely a result of the retarded autophagosome formation and/or transport (Fig. 7B). On the contrary, high levels of Atg8^{L55A}-PE were always detected even from cells maintained in nutrient-rich medium. Interestingly, the priming of nascent Atg8^{L55A} was not affected although it was catalyzed by the same Atg4 enzyme that mediated lipid deconjugation (Fig. 7C). Our results indicated that Atg8^{L55A} has a tendency to accumulate in cells as the PE-conjugated form.

In *atg1*Δ*atg8*Δ cells, unlike wild-type GFP-Atg8 that co-existed with RFP-Atg19 at a single PAS, GFP-Atg8^{L55A} frequently appeared at multiple puncta (Fig. 7D). Usually one of these structures colabeled with the RFP-tagged cargo receptor Atg19 reveling its PAS identity. Where the other GFP-Atg8^{L55A} located at remains to be analyzed and we were not able to co-localize them with other organelle markers, including the ER, Golgi and mitochondria (data not shown).

Discussion

In conventional membrane-trafficking pathways, the sorting and loading of cargo proteins are very often coupled with the coat protein-regulated vesicle formation processes.[34] Autophagy and its related pathways, on the other hand, have very different vesicle assembly mechanism by de novo generation of double membrane-bound structures in cytosol. Among the characterized autophagy regulatory proteins, Atg8 stands out by its lipidation and autophagosome association properties. In an *atg8*Δ strain, autophagy is inefficiently carried out suggesting the requirement of Atg8 for normal autophagosome formation.[29] Nakatogawa et al. recently conducted an in vitro study and found that Atg8 facilitates tethering and hemifusion of liposomes.[21] Abnormal long and unclosed isolation membrane structures, however, are observed in cells defective in Atg8/LC3 conjugation systems.[35,36] Hence the detailed in vivo mechanism underlying control of autophagosome formation by Atg8 remains to be confirmed. Regardless, Atg8 also participates in sorting and loading of selective autophagic cargo.[12,16] The Cvt pathway is induced by the major cargo prApe1 in vegetative growth yeast cells.[32] In line with this, protein aggregates likely stimulate their own elimination in mammalian neurons without the need of starvation stress. These observations suggest different regulatory mechanisms for cargo-induced selective autophagy versus starvation-triggered

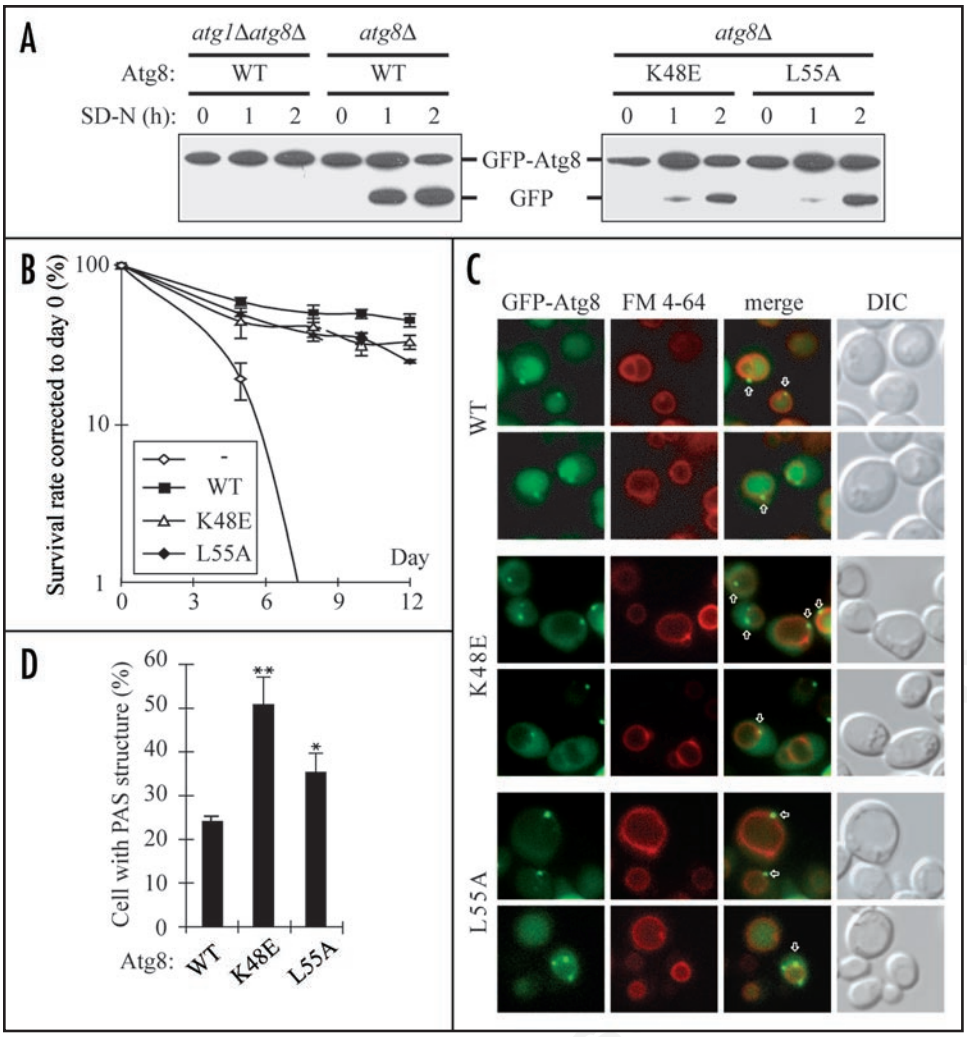

Figure 6. Characterization of Atg8^{K48E} and Atg8^{L55A} for autophagy activities. (A) Cells of an *atg8*Δ strain expressing GFP-Atg8, GFP-Atg8^{K48E} or GFP-Atg8^{L55A} were subjected to the GFP accumulation assay to analyze the progression of autophagy during starvation. (B) Cells of *atg8*Δ background harboring an empty vector or plasmids expressing Atg8 variants were tested for their survival rate in SD-N. The survival rate of each strain on day 0 was set to 100%. Error bars represent the standard deviations of three trials. (C) An *atg8*Δ strain expressing GFP-Atg8, GFP-Atg8^{K48E} or GFP-Atg8^{L55A} were stained with FM 4–64 and incubated in SD-N for 2 hours followed by microscopy observation. Arrows indicate PAS localized GFP-Atg8 variants. The percentages of cells exhibiting PAS-localized GFP-Atg8 variant signals were quantified (D). Error bars represent the standard deviations of three trials. In each trial, at least 100 cells were counted for each variant. Asterisks represent statistical difference between variants and wild type (*p < 0.05; **p < 0.005).

autophagy during early signaling processes. However, despite intensive studies on autophagy regulation and the machinery executing autophagosome formation, the mechanisms by which cargo evokes selective autophagy for its own transport and degradation are still elusive. Understanding how Atg8 coordinates vesicle formation and cargo sorting may shed light on studies of selective autophagy regulation.

By characterizing phenotypes of Atg8 variants, residue Arg28, Tyr49 and Leu50 of Atg8 were identified required for interaction with Atg19 (Fig. 3). Among these residues, Arg28 is positively charged. Atg8^{R28D} is defective in pulling down Atg19 and prApe1, which is consistent with the results indicating that the C-terminus of Atg19 with high density of acidic residues is responsible for interaction with Atg8 (Fig. 1). Ionic interactions, therefore, likely contribute to recognition and/or binding of Atg8 and Atg19. In addition, through statistic analysis of currently available structural information, arginine and partially exposed hydrophobic residues are found highly represented on interface of protein-protein interactions.[37] Our study not only identified Arg28, but also two other hydrophobic residues of Atg8, Tyr49 and Leu50, which are required for interaction with Atg19. These results indicate that Arg28-Tyr49-Leu50 likely constitute an Atg19-binding site on the surface of Atg8. While we were preparing this manuscript, two laboratories independently reported the p62-binding site of LC3.[38,39] Interestingly, several acidic and hydrophobic residues of p62 were found involved in interaction with partially surface-exposed hydrophobic residues of LC3. These LC3 residues are equivalent to Tyr49 and Leu50 of the yeast Atg8, suggesting Atg8 and its mammalian homologues share a conserved cargo-sorting mechanism to mediate selective autophagic transport.

Two previous reports and our current study have found that Lys48, Tyr49 and Leu50 are also required for execution of general autophagy transport.[21,22] Detailed analyses showed lipidation defect for Atg8^{Y49A}, but not for Atg^{K48E} and Atg8^{L50A} (Figs. 4 and 5). These three Atg8 mutants were all processed by Atg4 normally during initial priming. Our study further showed that they all could interact with the E1-like enzyme Atg7 more or less normally like wild-type Atg8. These data suggest that substitutions at these residues did not cause gross conformational alteration and the impairment of lipidation modification or autophagy regulation occurred at steps downstream to interaction with Atg7. Furthermore, despite of differences in accessibilities to lipid conjugation, both Atg8^{Y49A} and Atg8^{L50A} were not efficiently recruited to the PAS, whereas Atg8^{K48E} was seen localized at the PAS. This result indicates that lipidation alone is not sufficient for PAS-targeting of Atg8. Instead, interaction with transport cargo complex and/or deconjugation may play an important role in correct targeting of Atg8 to isolation membrane (see below).

Most unexpectedly, our study has characterized the cargo-receptor binding site of Atg8 to a region that is also important for autophagy regulation. This Atg19-binding site is in close proximity to the N-terminal helical domain (NHD) of Atg8 (Fig. 2). Several lines of evidence suggest that the NHD switches to an open conformation once Atg8 or its mammalian homologs is conjugated to a lipid

molecule.[40,41] Nakatogawa et al. proposed that this open conformation of Atg8 allows Atg8 to form multimers and to mediate membrane tethering and hemifusion.[21] Because the functional domains are partially overlapped, it will be interesting to test in the future if the presence of cargo-receptor Atg19 affects Atg8-mediated membrane tethering and hemifusion.

Additionally, the prApe1-Atg19 complex is known as a factor to induce the Cvt pathway but the exact regulatory mechanism is still elusive.[32] We tested whether the open conformation of lipid-conjugated Atg8 was required for its interaction with Atg19 and found that unmodified Atg8 can still pull down Atg19 (data not shown). Also, the generation of Atg8-PE during starvation is not affected in an *atg19*Δ strain, suggesting that selective cargo-binding is not a prerequisite for Atg8 lipidation, at least under starvation conditions. However, these results do not rule out the possibility that binding with Atg19 can in some extent affect lipid-conjugation or inhibit deconjugation of Atg8 especially during regulation of the Cvt pathway. In line with our results, we propose a model to explain the phenomenon of inducing selective autophagy by their transport cargo. The Atg19-binding site of Atg8 is close to the class II region (defined by Nakatogawa et al.[21]). Mutations at class II region lock Atg8 in lipidated form. Although the detailed mechanism of deconjugation regulation is still not clear, we hypothesize that Atg19-binding may hinder the class II region and prevent Atg8-PE deconjugation. Hence, Atg8-PE is kept membrane-associated at the PAS upon loading the prApe1-Atg19 complex into forming Cvt or autophagic transport vesicles. This model explains why GFP-Atg8 is usually not detected at the PAS in vegetative growing *ape1*Δ, *atg11*Δ or *atg19*Δ cells, which either lack of prApe1 or defective in targeting prApe1 to the PAS.[32]

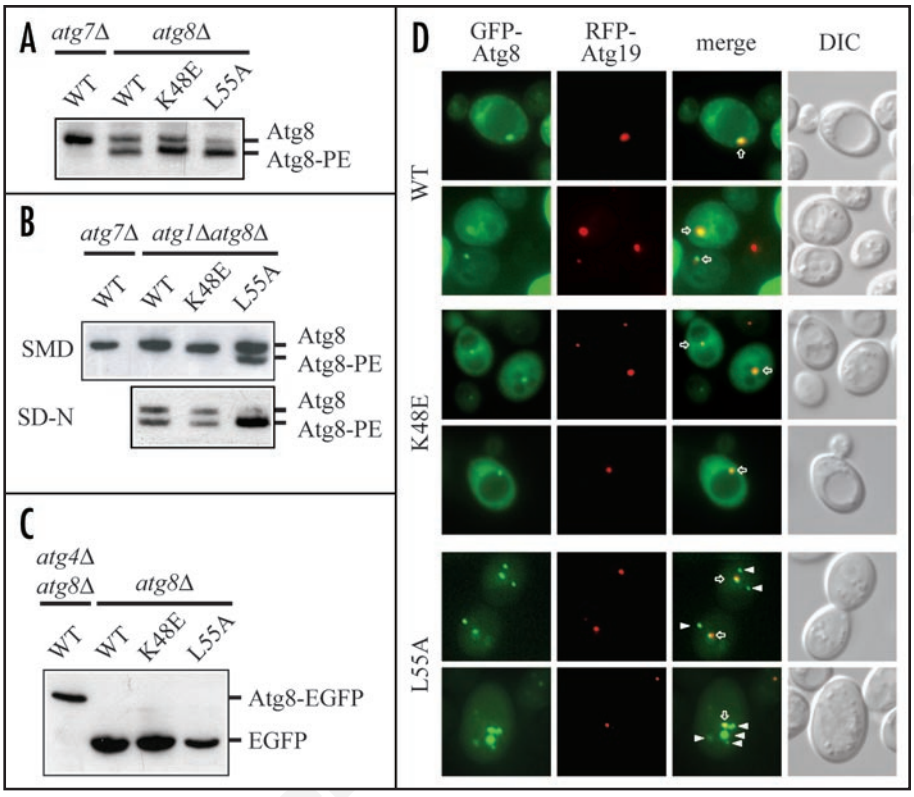

Figure 7. Analysis of Atg8^{K48E} and Atg8^{L55A} for processing defects. Plasmids expressing wild-type or Atg8 variants were transformed into (A) *atg7*Δ or *atg8*Δ, and (B) *atg1*Δ*atg8*Δ strains. Mid-log phase cells were subjected to Atg8 immunoblotting analysis for detecting lipidation. (C) The *atg8*Δ or *atg4*Δ*atg8*Δ strains expressing Atg8-EGFP, Atg8^{K48E}-EGFP or Atg8^{L55A}-EGFP were harvested at mid-log phase and subjected to immunoblotting analysis using anti-GFP antibodies. (D) The *atg1*Δ*atg8*Δ strain expressing RFP-Atg19 and the indicated GFP-Atg8 variants were grown to mid-log phase in SMD, shifted to SD-N for 2 hours, and then subjected to fluorescent microscopy. Arrows indicate PAS localized GFP-Atg8 variants; arrow heads represent GFP-Atg8^{L55A} that do not colocalize with RFP-Atg19.

The final autophagy regulation event involving Atg8 is its deconjugation catalyzed by Atg4, the same protease responsible for the initial priming step. Although this process is likely not related to selective cargo sorting, our study has identified an Atg8 mutant, Atg8^{Leu55A}, accumulated high level of lipid-conjugated form in vivo. Atg8^{L55A} was processed normally during priming event, suggesting it could still be recognized by Atg4. This, however, does not necessarily guarantee a normal Atg4-dependept deconjugation event for Atg8^{L55A} and why Atg8^{L55A} was kept as lapidated form in cells remains to be answered. We suspect that Atg8-PE associating with isolation membrane may be shielded by other regulatory proteins during autophagosome formation, and thus render the deconjugation recognition site of Atg8 inaccessible to Atg4. After the completion of autophagosome formation, disassembly and recycling of Atg proteins may expose Atg8-PE to Atg4 allowing deconjugation. This suspicion could explain our observation that an abnormally high level of lipid-conjugated GFP-Atg8^{L55A} proteins tended to mislocalize to multiple structures, and yet wild-type Atg8 only stably associates with the PAS. Atg4-dependent deconjugation could guarantee correct targeting of Atg8 to isolation membrane by releasing mislocalized Atg8 from other membrane structures where regulatory Atg proteins are missing to block deconjugation. The suspicion is consistent with our unpublished observation that the distribution of GFP-Atg8$^{\Delta R}$, an Atg8 variant with its C-terminal arginine residue deleted to bypass the initial priming event catalyzed by Atg4, in *atg4*Δ*atg8*Δ cells also showed tendency of mislocalization. It would be interesting to further confirm in the future if Atg8^{L55A} is defective in deconjugation event. Overall, our characterization of Atg8 mutants has not only defined a cargo-receptor binding site of Atg8 that is also important for the control of general autophagy transport, but also found many unexpected properties of Atg8. Further study of these Atg8 aspects should help us decipher the regulation mechanisms underlying selective autophagy.

Materials and Methods

Strains and media. The yeast *Saccharomyces cerevisiae* strains used in this study are listed in Table 1. Media used for growing yeast cells are as follows: SMD, 0.67% yeast nitrogen base without amino acid, 2% glucose, 0.5% casamino acid, auxotrophic amino acids and vitamins as need; SD-N, 0.17% yeast nitrogen base without amino acid

Table 1 **Yeast stains used in this study**

Strain	Genotype	Reference
SEY6210	*MATα his3-Δ200 leu2-3,112 lys2-801 trp1-Δ901ura3-52 suc2-Δ9 GAL*	Robinson et al., 1988
WPHYD7	SEY6210 *atg8Δ::LEU2*	Kim et al., 2001a
VDY101	SEY6210 *atg7Δ::LEU2*	Kim et al., 1999
SSY31	SEY6210 *atg19Δ::HIS5*	Scott et al., 2001
CCY7	SEY6210 *atg1Δ::HIS5 atg8Δ::KanMX*	Chang et al., 2007
WHY68	SEY6210 *atg4Δ::LEU2 atg8Δ::HIS3*	this study
WHY37	SEY6210 *atg1Δ::HIS5 atg4Δ::LEU2 atg8Δ::KanMX*	this study
PJ69-4A	*MATa trp1-Δ901 leu2-3,112 ura3-52 his3-Δ200 gal4Δ gal80Δ LYS2::GAL1-HIS3 GAL2-ADE2 met2::GAL7-lacZ*	James et al., 1996
WHY31	PJ69-4A *atg8Δ::TRP1*	this study
WHY4	PJ69-4A *atg19Δ::KanMX4*	Shintani et al., 2002
TN124	*MATα leu2-3,112 trp1 ura3-52 pho8::pho8Δ60 pho13Δ::LEU2*	Noda et al., 1995
WHY36	TN124 *atg8Δ::KanMX4*	this study
WHY42	TN124 *atg4Δ::TRP1 atg8Δ::KanMX4*	this study

and ammonium sulfate, 2% glucose, and vitamins as need; YPD, 1% yeast extract, 2% peptone, 2% glucose.

Plasmids. Plasmids expressing mutant Atg8 and Atg19 were generated with the QuickChange Site-Directed Mutagenesis kit (Stratagene, La Jolla, California) base on the plasmid pRS416-ATG8 and pRS416-ATG19.[12,23] For construction of plasmids expressing N-terminal protein A epitope (ProtA)-tagged or green fluorescent protein (GFP)-tagged Atg8 variants, EcoRI and SalI restriction sites were introduced by PCR to the ends of amplified *ATG8* open reading frame (ORF) with its endogenous transcription terminator. The resulting fragments were cloned into the corresponding restriction enzyme sites of pRS416-CuProtA and pRS416-CuGFP vectors.[9,24] For construction of the plasmid expressing red fluorescent protein (RFP)-Atg19 fusion, EcoRI and SalI sites were created by PCR to flank the ends of *ATG19* ORF with its endogenous transcription terminator. The amplified fragments were cloned into the corresponding restriction enzyme sites of pRS416-CuRFP vector. For construction of plasmids expressing C-terminal enhanced green fluorescent protein (EGFP)-tagged Atg8 variants, one PCR reaction was performed to amplify the *ATG8* ORF with an EcoRI site 204 base pair upstream of the *ATG8* start codon to include its endogenous promoter. The stop codon of *ATG8* ORF was also replaced by a 12 nucleotides sequence in this PCR, which is identical to the 5' end of EGFP coding sequence. Another PCR was performed to amplify EGFP ORF and to create an in frame stop codon followed by a SalI site just after this ORF. The resulting two PCR amplified fragments were mixed and used as the template to further PCR amplify the Atg8-EGFP coding sequence. The final PCR product was cloned into EcoRI and SalI sites of the pRS416 plasmid containing a CYC1 transcription terminator cassette. For construction of plasmids expressing $Atg8^{\Delta R}$, an EcoRI site was incorporated upstream of the promoter of *ATG8* and a new stop codon followed by a SalI site was created after its Gly116 codon by PCR to replace the Arg117 codon and the original stop codon. The resulting fragment was cloned into the EcoRI and SalI sites of pRS416 plasmid containing a CYC1 transcription terminator cassette. For construction of the two-hybrid analysis plasmids of ATG7 and ATG8, XmaI and ClaI sites were created to flank the *ATG7* ORF; BamHI and SalI sites were created to flank the *ATG8* ORF by PCR reactions. The amplified *ATG7* and *ATG8* ORF were cloned to the corresponding sites of pGAD-C2 and pGBDU-C2, respectively.[25] The two-hybrid analysis plasmids of Atg19 were described elsewhere.[12] For construction of charge-reversed ATG19 plasmid for the two-hybrid analysis, the corresponding ATG19 ORF were PCR amplified from pRS4-16-$ATG19^{-/+(6)}$ and subcloned to pGAD-C2 plasmid. All plasmids used in this study except those used for the two-hybrid analysis are yeast centromeric plasmids.

Homology-modeling and protein sequence alignment. The protein sequence alignment of Atg8 and its mammalian homologs was performed using the DNAMAN software. The homology-modeling of Atg8 was performed by the SWISS MODEL program (http://swissmodel.expasy.org/SWISS-MODEL.html)[26,27] using the solved structures of GATE-16 from Protein Data Bank as the comparative computing template. The predicted structure was presented by the Swiss-PdbViewer (http://www.expasy.org/spdbv).

Immunoblotting analysis. Cells grown to mid-log phase in SMD were harvested, precipitated by 10% TCA, and washed with acetone twice. Then the air-dried cell pellet was lysed in Laemmli sample buffer (125 mM Tris-Cl pH 6.8, 2% SDS, 15% glycerol, 0.005% bromophenol blue, 1% β-mercaptoethanol) by vigorous vortexing with silica beads (BioSpec Products, Inc., Bartlesville, Oklahoma) and boiled for 5 minutes. The total lysate was then subjected to sodium dodecyl sulfate-polyacrylamide gel electrophoresis (SDS-PAGE), transferred to polyvinylidene difluoride (PVDF) membrane, and blotted with the indicated antibodies. For separating the PE conjugated and non-conjugated forms of Atg8, a modified SDS-PAGE using a 12.5% polyacrylamide gel containing 6 M urea was performed following the described procedures.[11]

Protein A-pull down. Cells harvested at mid-log phase were converted to spheroplasts by Zymolyase 100T (Seikagaku Corporation, Tokyo, Japan) and lysed in PBS lysis buffer (1X phosphate buffered saline pH 7.4, 0.2 M Sorbitol, 5 mM $MgCl_2$, 0.5% Triton X-100) with EDTA-free complete protease inhibitor cocktail (Roche, Penzberg, Germany). The total lysate was centrifuged at 800 rpm for 5 minutes to remove unlysed cells. The resulting supernatant was collected and incubated with human IgG-coated

M-500 subcellular dynabeads (Invitrogen, Carlsbad, California) at 4°C overnight. Then, the beads were collected, washed with PBS lysis buffer 6 times and subjected to immunoblotting analyses using the indicated antibodies.

Yeast two-hybrid analysis. The yeast two-hybrid analysis was performed following the system established earlier.[25] Plasmids expressing the indicated fusion proteins or the corresponding Gal4 activation domain (AD) and DNA-binding domain (BD) were transformed into an *atg8*Δ yeast two-hybrid testing strain. The transformants were replicated to a SMD plate lacking histidine with 3 mM of 3-amino-1,2,4-triazole (3-AT) to analyze the interaction between the bait and the prey.

Assay of alkaline phosphatase (ALP) activity. The ALP assay was performed following the previously published system.[28] The *atg8*Δ and *atg4*Δ*atg8*Δ strains transformed by an empty vector or the indicated plasmids expressing Atg8 variants were grown to mid-log phase in SMD and switched to SD-N for 4 hours. Then, cells were harvested and lysed in lysis buffer (20 mM PIPES pH 6.8, 50 mM KCl, 100 mM KOAc, 10 mM $MgSO_4$, 10 μM $ZnSO_4$, 1 mM PMSF and 0.5% Triton X-100) by silica beads at 4°C. The prepared lysate was transferred to a 96-well microplate and incubated with 1 mM p-NPP (p-nitrophenol phosphate) as the substrate at 30°C for 30 min. The reaction was stopped by adding the stop buffer (1 M glycine pH 11). The relative activity of ALP was determined as following: dividing the A_{405} reading of a reaction by its own protein concentration measured by the BCA™ Protein Assay Kit (Thermo Fisher Scientific, Inc., Rockford, Illinois). The acquired values were then adjusted by setting the ALP activity of wild type to 100%.

Survival curve analysis. Cultures grown to mid-log phase in SMD were switched to SD-N. Aliquots of cells were then harvested from the culture on each indicated day and diluted to a suitable cell density. The cell suspension was plated to YPD plates and the colony numbers were counted after 2 days of incubation at 30°C. The survival rate in SD-N of a strain on each indicated day was determined as following: dividing the colony number on plates of the test day by the colony number of day 0 (prior to starvation treatment).

Fluorescence microscopy. Cells were harvested at mid-log phase and switched to SD-N for 2 hours. Cells were then collected, resuspended in distilled water, and smeared on slides for microscope observation. For FM 4–64 labeling, cells were incubated with 8 μM N-(triethylammoniumpropyl)-4-(p-diethylaminophenylhexatrienyl) pyridinium (FM 4–64) in YPD for 20 minutes and chased in YPD for another 30 minutes prior to starvation treatment. Fluorescence microscopy analyses were performed with a Zeiss Axioskop 2 plus fluorescent microscope equipped with an AxioCam CCD camera. Images were acquired with the AxioVision software.

Acknowledgements

We thank Drs. Daniel Klionsky (University of Michigan), Mark Longtine (Oklahoma State University), and Yoshinori Ohsumi (National Institute for Basic Biology, Japan) for supplying plasmids and strains. This work was supported by grant NSC95-2311-B-002-019-MY3 from the National Science Council of Taiwan (to W.-P. Huang).

References

1. Mizushima N, Levine B, Cuervo AM, Klionsky DJ. Autophagy fights disease through cellular self-digestion. Nature 2008; 451:1069-75.
2. Ogawa M, Yoshimori T, Suzuki T, Sagara H, Mizushima N, Sasakawa C. Escape of intracellular Shigella from autophagy. Science 2005; 307:727-31.
3. Nakagawa I, Amano A, Mizushima N, Yamamoto A, Yamaguchi H, Kamimoto T, Nara A, Funao J, Nakata M, Tsuda K, Hamada S, Yoshimori T. Autophagy defends cells against invading group A Streptococcus. Science 2004; 306:1037-40.
4. Gutierrez MG, Master SS, Singh SB, Taylor GA, Colombo MI, Deretic V. Autophagy is a defense mechanism inhibiting BCG and Mycobacterium tuberculosis survival in infected macrophages. Cell 2004; 119:753-66.
5. Komatsu M, Waguri S, Chiba T, Murata S, Iwata J, Tanida I, Ueno T, Koike M, Uchiyama Y, Kominami E, Tanaka K. Loss of autophagy in the central nervous system causes neurodegeneration in mice. Nature 2006; 441:880-4.
6. Hara T, Nakamura K, Matsui M, Yamamoto A, Nakahara Y, Suzuki-Migishima R, Yokoyama M, Mishima K, Saito I, Okano H, Mizushima N. Suppression of basal autophagy in neural cells causes neurodegenerative disease in mice. Nature 2006; 441:885-9.
7. Levine B, Klionsky DJ. Development by self-digestion: molecular mechanisms and biological functions of autophagy. Dev Cell 2004; 6:463-77.
8. Huang W-P, Klionsky DJ. Autophagy in yeast: a review of the molecular machinery. Cell Struct Funct 2002; 27:409-20.
9. Kim J, Huang W-P, Klionsky DJ. Membrane recruitment of Aut7p in the autophagy and cytoplasm to vacuole targeting pathways requires Aut1p, Aut2p and the autophagy conjugation complex. J Cell Biol 2001; 152:51-64.
10. Ichimura Y, Kirisako T, Takao T, Satomi Y, Shimonishi Y, Ishihara N, Mizushima N, Tanida I, Kominami E, Ohsumi M, Noda T, Ohsumi Y. A ubiquitin-like system mediates protein lipidation. Nature 2000; 408:488-92.
11. Kirisako T, Ichimura Y, Okada H, Kabeya Y, Mizushima N, Yoshimori T, Ohsumi M, Takao T, Noda T, Ohsumi Y. The reversible modification regulates the membrane-binding state of Apg8/Aut7 essential for autophagy and the cytoplasm to vacuole targeting pathway. J Cell Biol 2000; 151:263-76.
12. Shintani T, Huang W-P, Stromhaug PE, Klionsky DJ. Mechanism of cargo selection in the cytoplasm to vacuole targeting pathway. Dev Cell 2002; 3:825-37.
13. Hutchins MU, Klionsky DJ. Vacuolar localization of oligomeric alpha-mannosidase requires the cytoplasm to vacuole targeting and autophagy pathway components in *Saccharomyces cerevisiae*. J Biol Chem 2001; 276:20491-8.
14. Kim J, Scott SV, Oda MN, Klionsky DJ. Transport of a large oligomeric protein by the cytoplasm to vacuole protein targeting pathway. J Cell Biol 1997; 137:609-18.
15. Yorimitsu T, Klionsky DJ. Atg11 links cargo to the vesicle-forming machinery in the cytoplasm to vacuole targeting pathway. Mol Biol Cell 2005; 16:1593-605.
16. Chang C-Y, Huang W-P. Atg19 mediates a dual interaction cargo sorting mechanism in selective autophagy. Mol Biol Cell 2007; 18:919-29.
17. Bjorkoy G, Lamark T, Brech A, Outzen H, Perander M, Overvatn A, Stenmark H, Johansen T. p62/SQSTM1 forms protein aggregates degraded by autophagy and has a protective effect on huntingtin-induced cell death. J Cell Biol 2005; 171:603-14.
18. Kabeya Y, Mizushima N, Yamamoto A, Oshitani-Okamoto S, Ohsumi Y, Yoshimori T. LC3, GABARAP and GATE16 localize to autophagosomal membrane depending on form-II formation. J Cell Sci 2004; 117:2805-12.
19. Chen ZW, Chang CS, Leil TA, Olsen RW. C-terminal modification is required for GABARAP-mediated GABA(A) receptor trafficking. J Neurosci 2007; 27:6655-63.
20. Leil TA, Chen ZW, Chang CS, Olsen RW. GABAA receptor-associated protein traffics GABAA receptors to the plasma membrane in neurons. J Neurosci 2004; 24:11429-38.
21. Nakatogawa H, Ichimura Y, Ohsumi Y. Atg8, a ubiquitin-like protein required for autophagosome formation, mediates membrane tethering and hemifusion. Cell 2007; 130:165-78.
22. Amar N, Lustig G, Ichimura Y, Ohsumi Y, Elazar Z. Two newly identified sites in the ubiquitin-like protein Atg8 are essential for autophagy. EMBO reports 2006; 7:635-42.
23. Huang W-P, Scott SV, Kim J, Klionsky DJ. The itinerary of a vesicle component, Aut7p/Cvt5p, terminates in the yeast vacuole via the autophagy/Cvt pathways. J Biol Chem 2000; 275:5845-51.
24. Kim J, Huang W-P, Stromhaug PE, Klionsky DJ. Convergence of multiple autophagy and cytoplasm to vacuole targeting components to a perivacuolar membrane compartment prior to de novo vesicle formation. J Biol Chem 2002; 277:763-73.
25. James P, Halladay J, Craig EA. Genomic libraries and a host strain designed for highly efficient two-hybrid selection in yeast. Genetics 1996; 144:1425-36.
26. Schwede T, Kopp J, Guex N, Peitsch MC. SWISS-MODEL: An automated protein homology-modeling server. Nucleic Acids Res 2003; 31:3381-5.
27. Guex N, Peitsch MC. SWISS-MODEL and the Swiss-PdbViewer: an environment for comparative protein modeling. Electrophoresis 1997; 18:2714-23.
28. Noda T, Matsuura A, Wada Y, Ohsumi Y. Novel system for monitoring autophagy in the yeast *Saccharomyces cerevisiae*. Biochemical and biophysical research communications 1995; 210:126-32.
29. Abeliovich H, Dunn WA Jr, Kim J, Klionsky DJ. Dissection of autophagosome biogenesis into distinct nucleation and expansion steps. J Cell Biol 2000; 151:1025-34.
30. Paz Y, Elazar Z, Fass D. Structure of GATE-16, membrane transport modulator and mammalian ortholog of autophagocytosis factor Aut7p. J Biol Chem 2000; 275:25445-50.

31. Sugawara K, Suzuki NN, Fujioka Y, Mizushima N, Ohsumi Y, Inagaki F. The crystal structure of microtubule-associated protein light chain 3, a mammalian homologue of *Saccharomyces cerevisiae* Atg8. Genes Cells 2004; 9:611-8.
32. Shintani T, Klionsky DJ. Cargo proteins facilitate the formation of transport vesicles in the cytoplasm to vacuole targeting pathway. J Biol Chem 2004; 279:29889-94.
33. Tsukada M, Ohsumi Y. Isolation and characterization of autophagy-defective mutants of *Saccharomyces cerevisiae*. FEBS letters 1993; 333:169-74.
34. Aridor M, Traub LM. Cargo selection in vesicular transport: the making and breaking of a coat. Traffic 2002; 3:537-46.
35. Sou YS, Waguri S, Iwata J, Ueno T, Fujimura T, Hara T, Sawada N, Yamada A, Mizushima N, Uchiyama Y, Kominami E, Tanaka K, Komatsu M. The Atg8 conjugation system is indispensable for proper development of autophagic isolation membranes in mice. Mol Biol Cell 2008; 19:4762-75.
36. Fujita N, Hayashi-Nishino M, Fukumoto H, Omori H, Yamamoto A, Noda T, Yoshimori T. An Atg4B mutant hampers the lipidation of LC3 paralogues and causes defects in autophagosome closure. Mol Biol Cell 2008; 19:4651-9.
37. Zhou HX, Qin S. Interaction-site prediction for protein complexes: a critical assessment. Bioinformatics 2007; 23:2203-9.
38. Shvets E, Fass E, Scherz-Shouval R, Elazar Z. The N-terminus and Phe52 residue of LC3 recruit p62/SQSTM1 into autophagosomes. J Cell Sci 2008; 121:2685-95.
39. Ichimura Y, Kumanomidou T, Sou YS, Mizushima T, Ezaki J, Ueno T, Kominami E, Yamane T, Tanaka K, Komatsu M. Structural basis for sorting mechanism of p62 in selective autophagy. J Biol Chem 2008; 283:22847-57.
40. Ichimura Y, Imamura Y, Emoto K, Umeda M, Noda T, Ohsumi Y. In vivo and in vitro reconstitution of atg8 conjugation essential for autophagy. J Biol Chem 2004; 279:40584-92.
41. Coyle JE, Qamar S, Rajashankar KR, Nikolov DB. Structure of GABARAP in two conformations: implications for GABA(A) receptor localization and tubulin binding. Neuron 2002; 33:63-74.